JOURNAL OF CATALYSIS 144, 460–471 (1993)

Properties of Supported Pd–Ni Catalysts Prepared by Coexchange and by Organometallic Chemistry

I. Preparation and Characterization by X-Ray Diffraction, Analytical Microscopy, and EXAFS

J. F. FAUDON, F. SENOCQ,[1] G. BERGERET, B. MORAWECK, G. CLUGNET, C. NICOT, AND A. RENOUPREZ[2]

Institut de Recherches sur la Catalyse, CNRS, 2 Avenue Albert Einstein, F 69626 Villeurbanne Cedex, France

Received November 16, 1992; revised March 29, 1993

Silica-supported Pd–Ni bimetallic catalysts were prepared either by coexchange or via surface organometallic chemistry. In this later case, $Ni(C_5H_5)_2$ was allowed to react with a reduced Pd/SiO_2. The temperature of formation of the alloy was determined by *in situ* X-ray diffraction performed under flowing H_2 and the atomic order was determined by EXAFS. It is shown that the alloy is already formed at 620 K with organometallic precursors, whereas 840 K is necessary with coexchanged solids. A comparison between the X-ray methods and a careful analysis of the particle composition by EDX-STEM shows that the organometallic route leads to nearly homogeneous alloys. Alloy formation also occurs with coexchanged precursors; however, nickel in strong interaction with the support and unalloyed palladium are also observed.

INTRODUCTION

Bimetallic catalysts are widely used in catalytic reforming and in fine chemistry. Up to now, the reasons for choosing a given pair of metals have lain on an empirical basis. For example, the efficiency of the Pt–Re or Pt–Sn (*1*, *2*) associations in reforming catalysts was only explained *a posteriori*. Recent progress in surface science techniques, however, have led to a detailed knowledge of the composition, structure, and reactivity of the surfaces of alloys of platinum or palladium with nonnoble metals (*3*). It has been shown that two extreme situations can occur, leading either to minor modifications of the surface composition compared to that of the bulk, as in platinum alloys (*4*), or to a strong segregation of one of the components at the surface, which is the case for alloys of Pd with Fe, Ni, and Ag (*3*, *5*). However, since one of the driving forces leading to the segregation of one element is the surface tension, it is hazardous to extrapolate observations from bulk materials to fine particles. One of the purposes of this work is to understand of segregation in small particles.

Concerning the modifications of reactivity induced by alloying, the well-known concept of site dilution by an inactive metal can be invoked in a fairly large number of cases where, for example, a C–C bond rupture is concerned (*6*). Conversely, when two active metals are alloyed, a marked synergy is sometimes observed (*7*), which can be attributed to modifications of the ratio of the adsorption constants of the reactants and of the reaction products. Indeed, a correlation

[1] Present address: Laboratoire des Matériaux en Couches Minces, URA 445, Ecole Nationale Supérieure de Chimie, 118 Route de Narbonne, F 31077 Toulouse Cedex, France

[2] To whom correspondence should be addressed.

0021-9517/93 $5.00

between these modifications of the chemisorption properties of the alloy and the electronic structure of the noble metal could be established for the Pt–Ni, Pt–Fe, and Pd–Cr bimetallic systems (*5, 7, 8*). Little is known, however, on the reactivity of the Pd–Ni pair, two metals known for their activity in hydrogenation reactions.

Part I, the present paper, is devoted to the preparation and volume characterization of our catalysts, whereas Part II will concern their catalytic properties in relation to the surface composition determined by ESCA.

An essential condition which has to be fulfilled to perform this type of study is the obtaining of solids with homogeneous composition; simultaneous impregnation or coexchange of the two salts rarely leads to homogeneous solids. On the contrary, it is expected (*9*) that the decomposition of an organometallic compound can take place preferentially on metallic particles of the first metal, avoiding the formation of monometallic particles. Also, in most cases, the formation of the solid solution can only be verified *a posteriori*, after the preparation. A valuable help in the determination of the optimum conditions of thermal treatment leading to the formation of an alloy, used in the present study, is *in situ* X-ray diffraction performed under hydrogen.

EXPERIMENTAL

Sample Preparation

Silica-supported Pd–Ni catalysts were prepared by two different methods:

(*i*) *Cationic coexchange*. The silica support (Aerosil 200 Degussa) was treated in a 1 *N* ammonia solution to increase its exchange capacity. An aqueous solution of $Pd(NH_3)_4(OH)_2$ and $Ni(NO_3)_2 \cdot 6H_2O$ (Johnson–Matthey) was added to the carrier. The suspension, maintained at pH 10, was stirred for 24 h and the solvent was removed under vacuum in a revolving flask. The sample was then dried at 370 K for 15 h. Further treatments of calcination at 740 K and reduction under flowing hydrogen between 300 and 1000 K were performed either in the X-ray cell or in a preparation reactor.

(*ii*) *Preparation via organometallic route*. This was performed in two steps. A monometallic Pd catalyst was first prepared by the exchange method described above and nickelocene (bis-cyclopentadienyl-nickel, Aldrich) was decomposed on the surface in the presence of hydrogen. This reaction, studied by Pleass and Schimmel (*9*), can be written in the following way:

$$(C_5H_5)_2Ni + 2H_{ads} \rightarrow Ni + 2C_5H_6.$$

These authors have shown that the decomposition of the complex also takes place on the oxide, but one order of magnitude more slowly than on the metal. Moreover, a 2–5 h induction period is observed on oxides, whereas the reaction starts immediately and is completed within 1 h on metals. This difference can be attributed to the presence of chemisorbed hydrogen. Therefore, one can assume that nickel would be preferentially in contact with the palladium.

The nickelocene was purified by sublimation, and dissolved in dehydrated isoamylacetate (Aldrich) purified by fractional distillation. This solution was added under flowing argon to a suspension of reduced Pd/SiO_2 in isoamylacetate. The green suspension was stirred under flowing hydrogen at a temperature which was progressively raised from 300 to 390 K. This temperature was maintained until complete discoloration corresponding to the decomposition of the complex and formation of zerovalent nickel (*9*). After removal of the solvent, the catalyst was dried under vacuum at 320 K and transferred via a glove box to the X-ray diffraction oven or to the preparation reactor.

The main characteristics of the catalysts are gathered in Table 1, in which CE stands for coexchanged catalysts and OM for solids obtained via the organometallic route. The figure following the abbreviations represents the value of Pd at% on the basis of chemical analysis.

TABLE 1

Characteristics of the Coexchanged (CE) and Organometallic (OM) Catalysts

Sample	Composition (wt%)		Composition (at%) Pd	Reduction temperature (K)	Mean diameter (nm)
	Pd	Ni			
Pd/SiO_2	1.4	—	100	510	1.1[a]
CE21	1.4	2.9	21	840	2.8[a]
CE53	1.7	0.8	53	840	1.9[a]
CE71	3.0	0.7	71	840	3.1[a]
OM15	1.3	4.2	15	720	7.0[b]
OM40	2.7	2.3	40	720	4.0[b]
OM77	2.8	0.5	77	720	7.0[b]

[a] Measured by SAXS.
[b] Measured from the (111) diffraction linewidth.

X-Ray Diffraction

The *in situ* X-ray diffraction study of the alloy formation was performed on equipment including

—A Siemens X-ray generator delivering CuK_α radiation (Ni filtered, 1500 W).

—A Siemens D 500 goniometer set in the vertical position and bearing a horizontal oven. This homemade stainless steel oven is closed by a water-cooled cylindrical Be window and can be evacuated or flushed with dehydrated O_2, H_2, or He. The program-controlled temperature can reach 1000 K.

—A position-sensitive proportional counter (Raytech) filled with a flowing argon–methane mixture at 3 bar, which covers a 16° (2θ) angular range. The data acquisition, controlled by a microcomputer, can be performed with the counter in a fixed position or in a scanning mode if a larger angular range is needed. An evacuated collimator is fixed on the counter to eliminate the parasitic scattering produced by air and by the Be window. Compared to conventional X-ray equipments, using a scintillation detector and working in step-scanning mode, this detector improves the statistics by two orders of magnitude. Good quality spectra on weakly scattering materials such as a 2% Pd supported catalyst are recorded within 2 h. Including the spatial resolution of the detector (0.2 mm), the effect of parallax (which is the major factor), the size of the source, and the collimation effect, the instrumental resolution measured on a silicon powder was found to be 0.25° (2θ). This relatively low resolution does not broaden the structure including the (111) and (200) lines of a f.c.c. metal composed of 2–3 nm particles, which extends over 10°–12° (2θ). Actually, the quantitative analysis of such spectra, implying the subtraction of the support background, necessitates the recording of a 30° (2θ) angular range. A typical diffractogram is given in Fig. 1. A comparison between Figs. 1a and 1b shows that the scattering by the metal phase is only 20% of the total scattering; the background subtraction is however possible because the X-ray diagram of the support is structure free in the 30°–60° (2θ) range (Fig. 1c).

The lattice parameter increases by 10% from pure nickel to palladium (*10*). The Pd–Ni system forms a continuous solid solution over the whole range of concentration and constitutes a favourable case for diffraction studies. However, a lattice parameter cannot be measured straightforwardly from Fig. 1 since the (111) and (200) lines are not separated, as is well known for particles of 50–500 atoms (*11*). The appropriate data

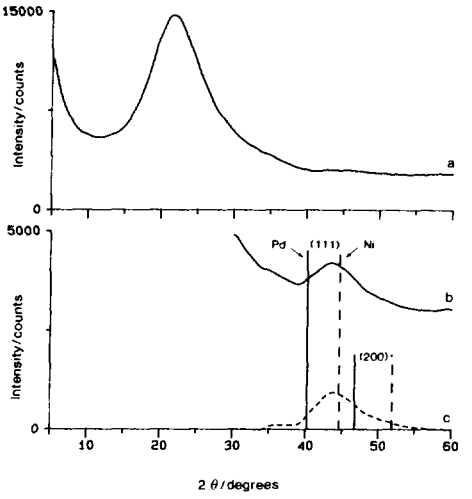

FIG. 1. X-ray patterns (a) of the silica carrier and of the CE21 sample after reduction (b) before and (c) after background subtraction. Vertical bars indicate the position of the Bragg peaks for palladium (full lines) and nickel (dashed lines) extracted from the JCPDS data set.

treatment would necessitate the fit of an intensity distribution (given by the Debye law) calculated for particles of discrete size and of different compositions, with the experimental profiles. Actually, after a background subtraction (Diffrac-AT software from SOCABIM), the global diffraction profile was simply adjusted to the sum of two Lorentzian functions describing the (111) and (200) profiles.

From the position of the (111) diffraction line, a unit cell parameter and thus a Pd atomic concentration can be determined with reference to the data of Bidwell and Speiser (*10*). The uncertainty of the alloy composition resulting from experimental errors and of the data treatment is estimated to ±3 at%.

Analytical Electron Microscopy

The distribution of composition of the particles was determined by scanning transmission electron microscopy (EDX-STEM) with a VG HB501 instrument using a probe of 0.5 nm diameter. For each sample, 20 to 30 particles were analyzed by measuring the PdL_α and NiK_α emission lines at 2.84 and 7.47 keV. The smallest particles were analyzed in spot mode with the beam in fixed position. The scanning mode on 3 × 3 or 10 × 10 nm^2 areas was used for large particles to improve statistics. Large areas (10^3 × 10^3 nm^2) of the support, where no particles were visible, were also scanned to verify the absence of atomically dispersed metal.

Besides the mean composition, $\langle x \rangle$, defined as

$$\langle x \rangle = \frac{\sum_i x_i n_i d_i^3}{\sum_i n_i d_i^3},$$

where x_i is the particle composition and n_i, the number of particles of diameter d_i. A mean quadratic deviation with respect to the composition, $\langle D \rangle$, was calculated by the relationship

$$\langle D \rangle = \sqrt{\frac{\sum_i n_i d_i^3 (x_i - \langle x \rangle)^2}{\sum_i n_i d_i^3}}.$$

Small Angle X-Ray Scattering

In situ SAXS experiments were performed with a goniometer equipped with an oven allowing treatment of the sample under hydrogen prior to the experiment. Difference experiments between the support and the catalyst led by application of the Porod law, to a metallic surface and to a surface weighted mean diameter. A particle diameter distribution and volume averaged diameter were also measured by this method (*12*).

X-Ray Absorption Experiments

The experiments were performed at the LURE synchrotron (Orsay, France) on the XAS4 station. The optics are composed of a Si (311) double crystal monochromator and of a double glass mirror to suppress the high order harmonics which are present at the Ni K edge. The transmission mode, with

Ar filled ion chambers detectors, was chosen to study the Pd K edge, whereas fluorescence, with Co filters (20 μm thick) and scintillation detector, was preferred for the Ni K edge because of the high absorption of palladium and silica at 8 keV. The spectra were recorded over 1000 eV at 3 eV intervals. At each energy, the counting time was 5 to 10 s obtained by summing 3 to 6 spectra. The data analysis has been explained in detail in a previous work (*8*). A fit was only attempted on the first coordination shell; the quality of this fit is expressed by a merit factor defined as

$$Q = \sum_i \frac{\{k^3[|\chi_i^c(k)| - |\chi_i^e(k)|]\}^2}{[k^3\chi_i^e(k)]^2},$$

where χ^c and χ^e are the calculated and experimental absorption normalized coefficients. Experimental backscattering amplitudes and phase shifts were measured from experiments on metal foils for the Pd–Pd and Ni–Ni pairs (*15* μm and 4 μm thick respectively) and extracted from the theoretical work of McKale *et al.* (*13*) for the mixed pairs.

In the case of bimetallic systems, EXAFS allows one to determine separately two mean coordination numbers around each type of metal atom A and B (n_{AA} and n_{AB} by an experiment at the A edge, n_{BA} and n_{BB} at the B edge); simultaneously, the corresponding bond lengths and Debye–Waller-like factors are calculated. If the quality of the data, of the treatment procedure, and of the phase shifts are satisfactory, one should, within the generally assumed precision (±0.02 Å), obtain equal values of R_{AB} and R_{BA}. Also, n_{BA} and n_{AB} are related to the atomic concentrations of A and B (c_A and c_B, respectively) in the system via the relationship $n_{AB}c_A = n_{BA}c_B = n_{BA}(1 - c_A)$ (*14*). This relation is strictly valid for an infinite network and it can happen that for very small particles it is not verified. Actually, its fulfilment would be the best criterion for the validity of the backscattering amplitudes.

When ordering occurs, the additional inequalities $n_{AA} < n_t c_A$ and $n_{AB} > n_t c_B$ (n_t is the total coordination number) would account for the tendency for an atom A to be mainly surrounded by B, as in the well known case of $AuCu_3$, for example. Also, information on a possible surface enrichment and on the surface composition can be drawn from the EXAFS data. Indeed, if the element A is mainly located in the outermost layer, the total coordination number should be appreciably lower around A than around B.

TABLE 2

Atomic Palladium Contents Measured by XRD and STEM Analysis

Sample	XRD	STEM
CE 21	13 (3)	55 (15)[a]
CE 53	32 (3)	58 (12)
CE 71	60 (3)	86 (5)[b]
OM 15	11 (3)	14 (5)
OM 40	36 (3)	42 (11)
OM 77	71 (3)	67 (5)

[a] Pure Ni particles are also observed.
[b] Pure Pd particles are also observed.

RESULTS AND DISCUSSION

STEM AND X-RAY DIFFRACTION

The analysis performed by STEM on a large sample area is in good agreement with the chemical analysis (±2%) for all the catalysts. This constitutes proof that the expression leading to the ratio of concentrations, which takes into account the ionization cross-sections and fluorescence yields, is correct, which ensures that the measurements on individual particles are reliable

CE Catalysts

The STEM analysis of selected particles and the X-ray diffraction results are summarized in Table 2.

Considering first the *CE21* sample, which has the larger Ni content, the X-ray pattern of Fig. 2a shows that after calcination, the only detected structure, around 35.5° (2θ), corresponds to a mixture of NiO and PdO.

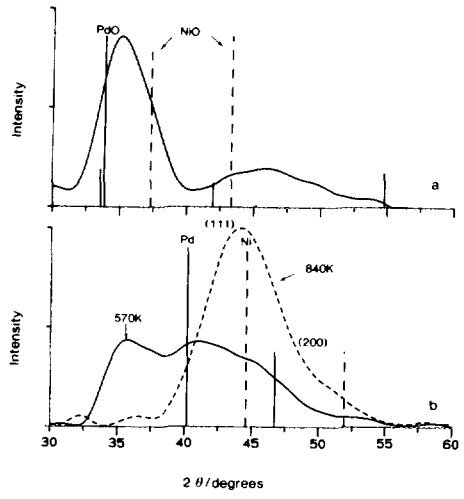

FIG. 2. CE21 sample: X-ray pattern after calcination (a) and after reduction (b) at 570 K (solid line) and 840 K (dashed line).

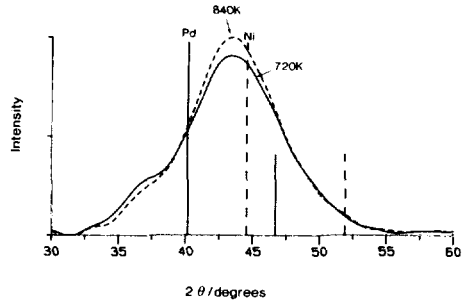

FIG. 3. CE53 sample: X-ray pattern after reduction at 720 K (solid line) and 840 K (dashed line).

The PdO line is still present at 570 K under hydrogen and disappears at 840 K (Fig. 2b). At 570 K a bimetallic phase is already present but the large width of the diffraction lines indicates that the solid solution is not homogeneous. It is noteworthy that at this relatively low temperature, part of the nickel has already been reduced, which is not the case for pure nickel on silica. This cooperative effect of a second metal has already been observed in the same system (*15*). Raising the temperature to 840 K eliminates the remaining NiO and the shift of the maximum of the diffraction line indicates that more nickel has been incorporated into the alloy.

For the CE53 sample, as shown in Fig. 3, no marked modification of the diffractogram can be observed between 720 and 840 K under hydrogen. The analysis of this last spectrum leads to a Pd concentration of 0.30 to 0.35 instead of 0.53, as obtained from the chemical analysis. The particle diameter deduced from the linewidth at the end of thermal treatment agrees with the diameter measured by SAXS, 1.9 nm.

On the CE71 sample, only PdO is detected after calcination (Fig. 4a). If present, NiO cannot be detected because of the low nickel loading and/or the formation of a dispersed nickel silicate. At 570 K under hydrogen (Fig. 4b), a limited amount of alloy is already found, but as the diffraction line is asymmetric, one cannot rule out the presence of pure

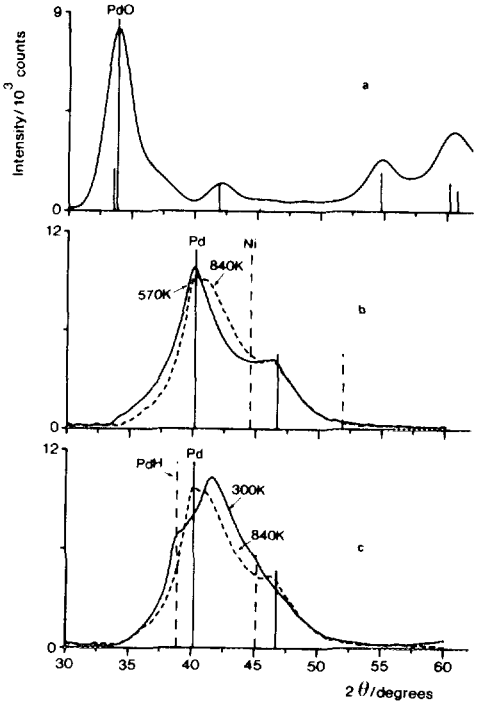

FIG. 4. CE71 sample X-ray pattern (a) after calcination at 740 K (vertical bars indicate the position of the Bragg peaks for palladium oxide); (b) after reduction at 570 K (solid line) and 840 K (dashed line); (c) under hydrogen at 840 K (dashed line) and after subsequent cooling at 300 K (solid line).

metallic phases. The X-ray diffraction pattern recorded at 840 K (Fig. 4b) seems to indicate a nickel enrichment of the bimetallic phase and the presence of unalloyed palladium. This is unambiguously confirmed by the observation of the Pd hydride diffraction line (Fig. 4c), when this sample is contacted with hydrogen at 300 K. From the main diffraction line of this pattern the mean composition of the alloy has been found to be $Pd_{60}Ni_{40}$.

In the STEM analysis on selected areas, the mean squared deviation with respect to the mean composition is for all samples 10% to 15%. However, in all cases, a discrepancy between STEM, X-ray diffraction results, and chemical analysis (CA) is observed. In samples like CE71, the divergence is not very large. For the CE21 catalyst, in contrast, the 3 × 3 nm^2 area analyzed by the microscope shows the presence of a Pd-rich alloy and of particles of unalloyed Ni. However, the main reason for the discrepancy between STEM and CA is the fact that the smallest particles, with a diameter smaller than 1.5 nm, are hardly visible and are probably not taken into account in the EDX analysis. This is especially the case if they are nickel-rich, because of the poor contrast between silica and nickel.

Finally, the solid solutions observed by diffraction are palladium-deficient, with the corollary that ultrafine Pd particles, undetected by STEM and X-ray diffraction, should also be present. Only when the Pd concentration is large (sample CE71) is a Pd phase observed by X-ray diffraction. An alternative explanation for the low Pd concentration measured by diffraction compared to CA for CE53 and CE21 could be the presence of non-f.c.c. particles. Indeed, the shape of the diffraction lines observed in Figs. 2 and 3 looks very similar to the shape of those reported by Hall *et al.* (*16*) in the case of unsupported silver particles which were studied by electron diffraction. These authors showed that for particle diameters of 4 to 5 nm, icosahedral and decahedral domains produce much broader diffraction lines than f.c.c. particles, with no separation between the first two lines and an apparent shift toward large 2θ values.

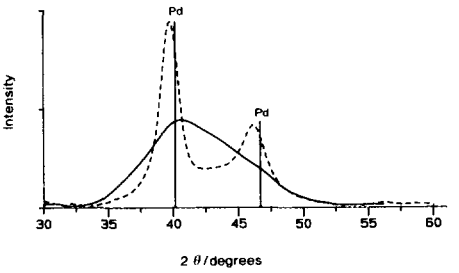

FIG. 5. Pd on silica sample (2.8 wt%): X-ray pattern before (solid line) and after (dashed line) isoamylacetate introduction.

OM Samples

In Fig. 5, the effect of introducing the isoamylacetate solvent on the Pd/SiO_2 catalyst can be observed. Indeed, after reduction at 510 K, a coalescence of the particles and a crystallographic reorganisation have occurred. Their mean diameter is increased from 1.9 to 4 nm. The slight shift of the diffraction lines toward low angles with respect to bulk palladium can be attributed to the incomplete decomposition of the hydride at 510 K.

In the diagrams represented in Figs. 6a, b, and c, the first two diffraction lines are now well apart and the concentration of Pd in the solid solutions is close to the value obtained from the CA.

For the OM15 and OM77 samples (Figs. 6a and c), the (111) and (200) diffraction lines are already well identified at 490 K. Heating under H_2 at 620 K modifies the composition of the alloy, which is Pd-enriched for OM15 and Ni-enriched for OM77. Finally at 720 K, the line width corresponds to particles with a diameter of 7 nm. This is a direct proof that the alloy has a uniform composition. In contrast, the larger linewidth observed in Fig. 6b for OM40 is an indication of a composition distribution.

The analysis by STEM was hindered by the presence of strings of particles which in

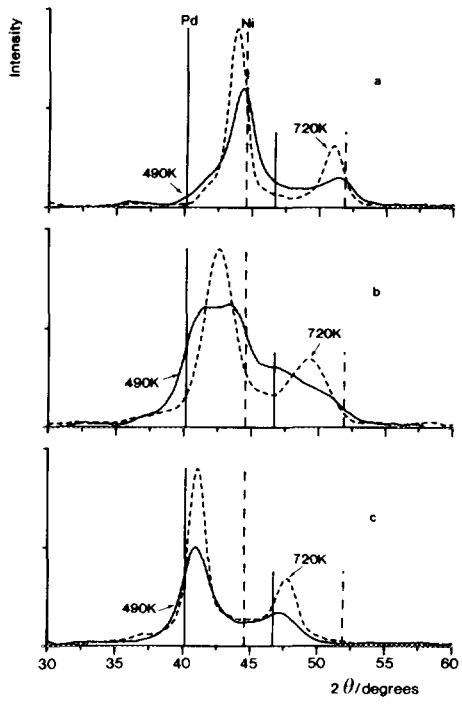

FIG. 6. X-ray pattern after reduction at 490 K (solid line) and 720 K (dashed line): (a) OM15 sample; (b) OM40 sample; (c) OM77 sample.

some cases prevent the analysis of isolated particles, but it confirms that all the metal is located in the $10 \times 10\ nm^2$ selected areas. All these results show that this method of preparation leads to homogeneous solid solutions with no pure metal particles.

X-ray diffraction and STEM, however, are not able to determine the order on the atomic scale, especially if some surface segregation is present. An EXAFS study at both edges was thus undertaken.

X-Ray Absorption Study

The results concerning only the Pd edge for the CE samples and both edges for the OM samples are gathered in Tables 3, 4, and 5 and are illustrated in Figs. 7 to 10. The following remarks can be drawn from these results.

CE Samples

Despite several attempts, the modeling of the EXAFS spectra taken at the Ni *K* edge was not possible for the CE samples. As can be seen in Fig. 7, the nickel *K* edge structure of the CE71 sample is quite different from that of the reference Ni foil and close to that of nickel oxide. The Fourier transform (FT) corresponding to the CE71 sample (Fig. 8a) clearly contains Ni–O distances and the magnitude of this peak indicates the presence of an appreciable proportion of nickel in interaction with oxygen. This also holds for the other two CE samples. By comparison with the diffraction results described above, which do not detect noticeable amounts of oxides, the best explanation is that EXAFS is sensitive to bonds between nickel and oxygen atoms of the silica. Therefore, the presence of nickel silicate cannot be discarded.

At the Pd *K* edge (Figs. 8b and c), the coordination number for the pure Pd/SiO_2

TABLE 3

CE Samples: EXAFS Results at the Pd *K* Edge

Sample	Pd–Pd pairs			Pd–Ni pairs			$Q(\%)$	$n_1 + n_2$
	n_1	R_1(Å)	$\Delta\sigma^2$	n_1	R_2(Å)	$\Delta\sigma^2$		
Pd foil	12	2.75	—	—	—	—	—	—
Pd/SiO_2	6.3	2.76	0.005	—	—	—	9	—
CE 21	6.9	2.70	0.003	1.6	2.72	—	6	8.5
CE 53	3.5	2.72	0.005	4.7	2.63	0.014	5	8.2
CE 71	8.3	2.71	0.005	1.3	2.67	0.006	7	9.6

TABLE 4

OM Samples: EXAFS Results at the Pd *K* Edge

Sample	Pd–Pd pairs			Pd–Ni pairs			$Q(\%)$	$n_1 + n_2$
	n_1	R_1(Å)	$\Delta\sigma^2$	n_2	R_2(Å)	$\Delta\sigma^2$		
Pd foil	12	2.75	—	—	—	—	—	—
Pd/SiO_2	6.3	2.76	0.005	—	—	—	9	—
OM 15	1.5	2.70	0.000	9.3	2.57	0.008	12	10.8
OM 40	5.0	2.70	0.006	5.5	2.61	0.006	9	10.5
OM 77	8.3	2.70	0.004	2.4	2.67	0.010	12	10.7

catalyst is 6.3, in agreement with the particle diameter of 1.1 nm measured by SAXS (Table 3). For all the bimetallic samples, the total coordination number, $n_1 + n_2$, lies between 8.2 and 9.6, a consequence of the higher reduction temperature (840 K) than in the case of pure Pd. Note also that one finds a larger number of Pd neighbours around Pd than is expected from CA. This is especially the case for Ni-rich samples such as CE21 and is a consequence of the presence of nickel atoms bonded to oxygen, which cannot directly interact with palladium atoms.

Finally, one must conclude that the local order measured by EXAFS, especially when limited to the first neighbours, can hardly be compared with the long range order measured by diffraction. Also, the presence of several phases makes the EXAFS analysis questionable.

OM Samples

The first important remark is that Ni–O distances are no longer observed on the FT's of the OM samples (Fig. 9), a difference from the CE samples. A second important remark is that the independent fits at the two edges (Figs. 9 and 10) lead, within 0.03 Å, to the same distances for the Pd–Ni and the Ni–Pd pairs. Also, the total coordination number $n_1 + n_2$ varies between 10.5 and 10.8, which, for f.c.c. cuboctahedral clusters, corresponds to particles of 1000 to 3000 atoms (*17*) with a size of 4 to 5 nm for pure palladium. This is in reasonably good agreement with XRD results (Table 1), considering the uncertainties in the measurements. Note also that no substantial difference can be observed between the total coordination numbers, whether Pd or Ni is the probed atom. The consequence is that after a treatment at 720 K, no segregation

TABLE 5

OM Samples: EXAFS Results at the Ni *K* Edge

Sample	Ni–Pd pairs			Ni–Ni pairs			$Q(\%)$	$n_1 + n_2$	d(Å)
	n_1	R_1(Å)	$\Delta\sigma^2$	n_2	R_2(Å)	$\Delta\sigma^2$			
Ni foil	—	—	—	12	2.49	—	—	—	—
OM 15	1.3	2.57	0.004	9.3	2.49	0.000	2	10.6	2.53
OM 40	6.4	2.61	0.014	4.4	2.48	0.000	9	10.8	2.60
OM 77	9.5	2.64	0.017	1.3	2.44	0.000	24	10.8	2.69

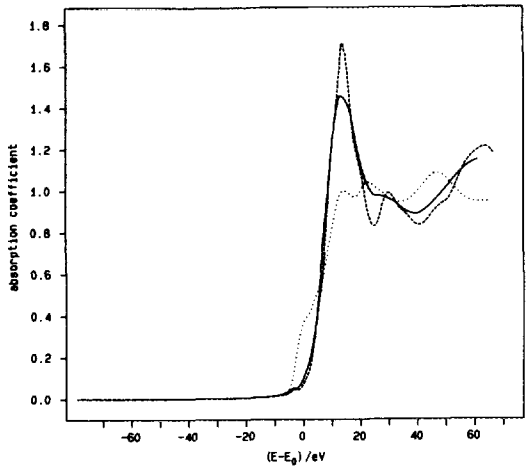

FIG. 7. X-ray absorption edge structure of metallic nickel (dotted line), nickel oxide (dashed line), and CE71 sample (solid line).

of one of the elements at the surface can be observed.

Finally, from the relationship between concentrations c and coordination numbers n, $c_A n_{AB} = c_B n_{BA} = (1 - c_A) n_{BA}$ (*14*), one obtains 0.13, 0.53, and 0.80 for the palladium concentration for the OM 15, 40, and 77 samples, respectively. The agreement with the chemical analysis is extremely good for the two extreme concentrations and these catalysts can be considered as true homogeneous alloys, even on the atomic scale. For the OM40 sample, as mentioned above, the diffraction lines are broader, the mean deviation with respect to the mean composition measured by STEM is 11% instead of 5% for the other samples, and the local Pd concentration measured by EXAFS is 30% larger than that obtained from the CA. This might be the indication of a tendency for this sample to be ordered at this composition. Another explanation could be variations of composition inside the particles.

A final interesting piece of information drawn from the EXAFS results is the comparison between the mean first neighbours distance extracted from the diffraction data, using the position of the (111) Bragg peak (d in the last column of Table 5), and the Pd–Pd, Pd–Ni, and Ni–Ni distances (Tables 4 and 5). The picture is a double coordination sphere around Ni atoms with Ni–Ni distances comparable to that of pure nickel

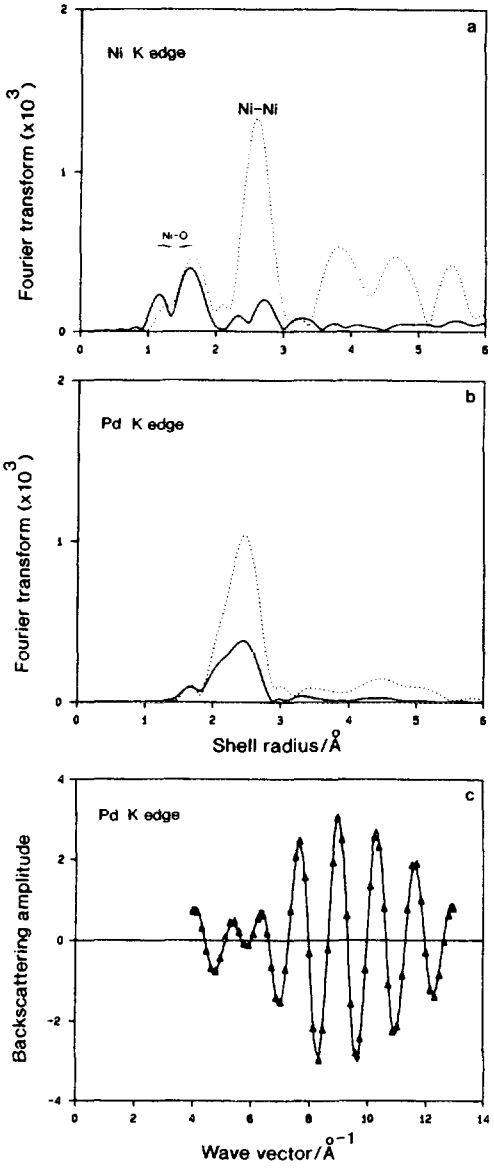

FIG. 8. CE71 sample: (a) Fourier transforms of the sample (solid line) and standard nickel oxide (dotted line) at the Ni K-edge; (b) Fourier transform of the sample (solid line) and standard Pd foil (dotted line) at the Pd K-edge; (c) first shell experimental (triangles) and modeled (solid line) contributions at the Pd K-edge.

(2.492 Å), shorter than the mean distance, and longer Ni–Pd bond lengths close to the mean distance. Around palladium, an expanded coordination sphere is observed, with a Pd–Pd bond length close to that of pure palladium (2.751 Å).

CONCLUSIONS

The observations on CE samples are an illustration of the difficulties encountered when one tries to compare the results of different methods of characterization if the samples are not homogeneous. Obviously the STEM analysis suffers from a lack of statistics and hardly takes into account the smallest particles. Concerning EXAFS and diffraction, the discrepancies can be ascribed to differences between short and long range order.

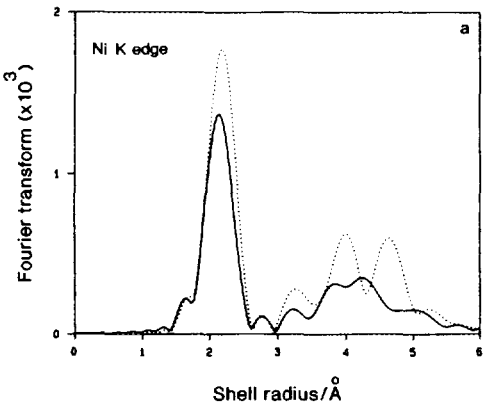

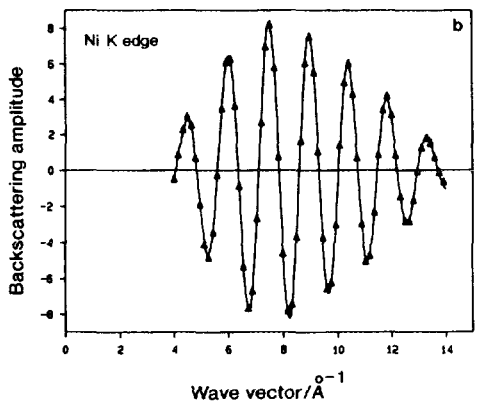

FIG. 9. OM15 sample at the Ni *K*-edge: (a) Fourier transform of the sample (solid line) and standard Ni foil (dotted line); (b) first shell experimental (triangles) and modeled (solid line) contributions.

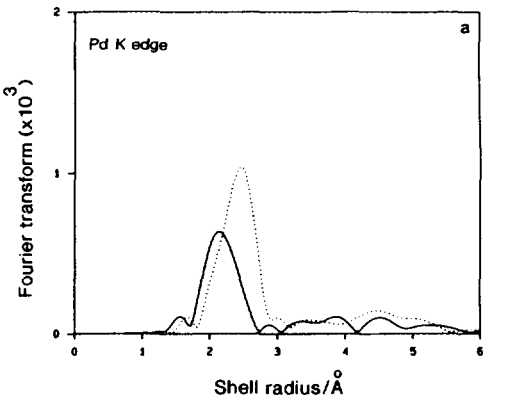

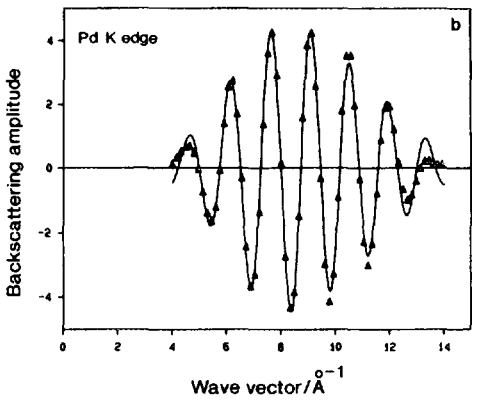

FIG. 10. OM15 sample at the Pd *K*-edge: (a) Fourier transform of the sample (solid line) and standard Pd foil (dotted line); (b) first shell experimental (triangles) and modeled (solid line) contributions.

As expected and known from the literature, the preparation of bimetallic solids by coexchange does not lead to homogeneous solid solutions when one of the metals is difficult to reduce or can form chemical combinations with the support. This is clearly the case of the CE samples which, beside alloy phases, are composed of nickel in interaction with the silica and pure palladium. On the contrary, the new preparation procedure (OM samples), consisting of reacting the nickel organometallic compound with prereduced palladium in the presence

of hydrogen, prevents the formation of unreduced nickel.

An important point is that at the temperature where a homogeneous solid solution is formed (720 K), no marked Pd surface enrichment is detected by EXAFS. This phenomenon was in contrast observed by the authors of Refs (*3*, *5*) for samples prepared above 900 K.

The good homogeneity of the OM samples is perfectly explained by the nucleation-growth theory. Following the ideas developed by Hamilton and Logel (*18*), the formation of aggregates on a support by vapour deposition of metal atoms proceeds in two steps: a limited number of nuclei are first formed on the defects of the support, and in a second step, larger aggregates grow from these nuclei to form three-dimensional particles. All the acidic sites of the silica are nearly saturated by the palladium complex, and after reduction, are no longer available to bond the nickel organometallic complex. Moreover, the decomposition and reduction of the nickel complex is catalytically assisted by the palladium and does not take place on the support.

ACKNOWLEDGMENTS

The authors are much indebted to O. Heckmann for his participation in the synchrotron data collection and to the Laboratoire pour l'Utilisation du Rayonnement Electromagnétique (LURE-ORSAY) for dedicated runs.

REFERENCES

1. Biswas, J., Bickle, G. M., Gray, P. G., Do, D. D., and Barbier, J., *Catal. Rev. Sci. Eng.* **30,** 161 (1988).
2. Sachdev, A., and Schwank, J., *in* "Proceedings, 9th International Congress on Catalysis, Calgary, 1988" (M. J. Phillips and M. Ternan, Eds.), Vol. 3, p. 1275. Chem. Inst. Canada, Ottawa, 1988.
3. Bertolini, J. C., Debauge, Y., Delichère, P., Massardier, J., Rousset, J. L., Ruiz, P., and Tardy, B., *in* "Proceedings, 10th International Congress on Catalysis, Budapest, 1992" (L. Guczi, F. Solymosi, and P. Tetenyi, Eds.), p. 66. 1992.
4. Abon, M., Massardier, J., Tardy, B., and Bertolini, J. C., *Surf. Sci* **189,** 880 (1987).
5. Mintsa-Eya, V., Hilaire, L., Touroude, R., Gault, F. G., Moraweck, B., and Renouprez, A., *J. Catal.* **76,** 169 (1982).
6. Sinfelt, J. H., *Catal. Letters.* **9,** 159 (1991).
7. Renouprez, A. J., Moraweck, B., Imelik, B., Perrichon, V., Dominguez, M., and Jablonski, J., *in* "Proceedings, 7th International Congress on Catalysis, Tokyo, 1980" (T. Seiyama and K. Tanabe, Eds.), Vol. A8, p. 173. Elsevier, Amsterdam, 1981.
8. Borgna, A., Moraweck, B., Massardier, J., and Renouprez, A. J., *J. Catal.* **128,** 99, (1991).
9. Pleass, C. M., and Schimmel, D. G., *J. Catal.* **24,** 424, (1972).
10. Bidwell, L. R., and Speiser, R., *Acta Crystallogr.* **17,** 1473 (1964).
11. Gallezot, P., Avalos-Borja, M., Poppa, H., and Heinemann, K., *Langmuir* **1,** 342 (1985).
12. Espinat, D., Moraweck, B., Larue, J. F., and Renouprez, A., *J. Appl. Crystallogr.* **17,** 269 (1984).
13. McKale, A. G., Veal, B. W., Paulikas, A. P., Chan, S.-K., and Knapp, G. S., *J. Am. Chem. Soc.* **110,** 3763 (1988).
14. Via, G. H., Drake, K. F., Meitzner, G., Lytle, F. W., and Sinfelt, J. H., *Catal. Lett.* **5,** 25 (1990).
15. Shaefer Feeley, J., and Sachtler, W. M. H., *Zeolites* **10,** 738 (1990).
16. Hall, B. D., Flueli, M., Monot, R., and Borel, J. P., *Phys. Rev. B* **43,** 3906 (1991).
17. Gordon, M. B., Ph.D. Thesis, Grenoble, 1978.
18. Hamilton, J. F., and Logel, P. C., *Thin Solid Films* **16,** 49 (1973).